Dissipation-Driven Superradiant Phase Transition of a Two-Dimensional Bose–Einstein Condensate in a Double Cavity

Bo-Hao Wu[1,2], Xin-Xin Yang[1,2], Yu Chen[3*], and Wei Zhang[1,2,4*]

[1]*Department of Physics and Beijing Key Laboratory of Opto-electronic Functional Materials and Micro-nano Devices, Renmin University of China, Beijing 100872, China*
[2]*Key Laboratory of Quantum State Construction and Manipulation (Ministry of Education), Renmin University of China, Beijing 100872, China*
[3]*Graduate School of China Academy of Engineering Physics, Beijing 100193, China*
[4]*Beijing Academy of Quantum Information Sciences, Beijing 100193, China*

(Received 20 February 2024; accepted manuscript online 28 April 2024)

We study superradiant phase transitions in a hybrid system of a two-dimensional Bose–Einstein condensate of atoms and two cavities arranged with a tilt angle. By adjusting the loss rate of cavities, we map out the phase diagram of steady states within a mean field framework. It is found that when the loss rates of the two cavities are different, superradiant transitions may not occur at the same time in the two cavities. A first-order phase transition is observed between the states with only one cavity in superradiance and both in superradiance. In the case that both cavities are superradiant, a net photon current is observed flowing from the cavity with small decay rate to the one with large decay rate. The photon current shows a non-monotonic dependence on the loss rate difference, owing to the competition of photon number difference and cavity field phase difference. Our findings can be realized and detected in experiments.

DOI: 10.1088/0256-307X/41/6/064201

Strong coupling between ultracold atoms and electromagnetic field in cavities provides us with a platform to study various interesting many-body collective phenomena.[1–3] Meanwhile, it also promotes advanced development of theory and experiment regarding steady state superradiance.[4–8] In recent years, superradiant phase transition in multiple cavity modes has been proposed and investigated,[9–13] with particular interests on the phase diagram and symmetry analysis. Moreover, the dynamics of Higgs and Goldstone modes have also been observed in multiple cavity systems.[14]

One key characteristic of the atom-cavity hybrid system is that the atoms are in a dynamical steady state under simultaneous pumping and decay. The presence of cavity dissipation can bring in structural instability and abnormal dynamics in a Bose–Einstein condensate (BEC).[15–17] Multi-critical phenomena induced by dissipation have been witnessed due to the anomalous quantum fluctuations.[18] By controlling the competition between coherent dynamics and dissipation, the dissipative phase could be achieved.[19] It is then of great interest to discuss influence of dissipation on superradiant phase transitions in multiple cavity systems.

In this Letter, we consider a two-dimensional (2D) BEC of neutral atoms loaded inside two cavities, and study the influence of unbalanced cavity loss rates on superradiant transitions within the mean field framework. We find that by tuning the difference of cavity loss rate of the two cavities, two superradiant phases can be stabilized: one cavity in superradiance phase and one in normal phase (SR-I), and two cavities are both in superradiance phase (SR-Ⅱ). The two superradiance phases are separated by a first-order phase transition, and will change to the normal phase via a second-order phase transition. The two second-order transition lines join with the first-order transition at a tetra-critical point. Thus, a rich phase diagram with different types of phase transition can be realized by controlling pumping and dissipation. Furthermore, we calculate the net photon current between the two cavities in the SR-Ⅱ region, and find a nontrivial dependence on the loss rate difference, owing to the competition between the cavity photon number and the phase difference between cavity modes. We also provide an experimental proposal for measuring the intra-cavity photon current.

In the following, we first introduce the theoretical model of the double-cavity system and the formalism to solve the steady state equation of atoms and cavity photons. Then, the main results of superradiance phase diagram and photon current between cavities are discussed. Finally, we discuss possible experimental realizations and summarize the results.

Model and Mean Field Treatment. We consider a 2D BEC of atoms loaded inside two optical cavities that cross at an angle of θ in the x–y plane. The two cavities are set

*Corresponding authors. Email: ychen@gscaep.ac.cn; wzhangl@ruc.edu.cn
© 2024 Chinese Physical Society and IOP Publishing Ltd

along the $\hat{x}$ and $\cos\theta\hat{x}+\sin\theta\hat{y}$ directions, and the pumping beam is applied along the $\hat{z}$ direction (see Fig. 1). The cavity fields are linearly polarized and are assumed to be resonant with the same frequency $\omega_{\rm c}$ and wavelength λ, while the pumping field with frequency $\omega_{\rm p}$ is circularly polarized. By eliminating the atomic excited states and applying the rotating-wave approximation, the Hamiltonian reads (with natural units $\hbar = k_{\rm B} = 1$)

$$\hat{H} = \int d\boldsymbol{r}\ \hat{\Psi}^{\dagger}(\boldsymbol{r})\hat{H}_0\hat{\Psi}(\boldsymbol{r}) - \Delta_{\rm c}\sum_{j=1}^{2}\hat{a}_j^{\dagger}\hat{a}_j, \tag{1}$$

$$\hat{H}_0 = \frac{p_x^2+p_y^2}{2m} + \eta_0\sum_{j=1}^{2}\cos(\boldsymbol{k}_j\cdot\boldsymbol{r})(\hat{a}_j+\hat{a}_j^{\dagger}) + U_0\sum_{m,n=1}^{2}\cos(\boldsymbol{k}_m\cdot\boldsymbol{r})\cos(\boldsymbol{k}_n\cdot\boldsymbol{r})\hat{a}_m^{\dagger}\hat{a}_n. \tag{2}$$

Here, $\hat{\Psi}(\boldsymbol{r})$ is the bosonic field operator for the BEC and m is the atomic mass. The cavity fields are denoted by $\hat{a}_j$ and $\hat{a}_j^{\dagger}$ with $j = 1, 2$ labeling the cavities. The wave vectors of the cavity fields are $\boldsymbol{k}_1 = k_0\hat{x}$ and $\boldsymbol{k}_2 = k_0(\cos\theta\hat{x}+\sin\theta\hat{y})$, with the same wave number $k_0 = 2\pi/\lambda$. The cavity modes are detuned from the pumping laser by $\Delta_{\rm c} = \omega_{\rm p} - \omega_{\rm c}$. The depth of cavity self-energy potential is denoted as $U_0 = g_0^2/\Delta_{\rm a}$, where g_0 represents the atom-cavity coupling strength and $\Delta_{\rm a} = \omega_{\rm p} - \omega_{\rm a}$ represents the atom-light detuning, with $\omega_{\rm a}$ being the atomic transition frequency. The effective pumping strength is $\eta_0 = g_0\Omega_0/\Delta_{\rm a}$, with Ω_0 the Rabi frequency of pumping laser. In the following discussion, we use the recoil energy $E_{\rm r} = k_0^2/2m$ as the energy unit.

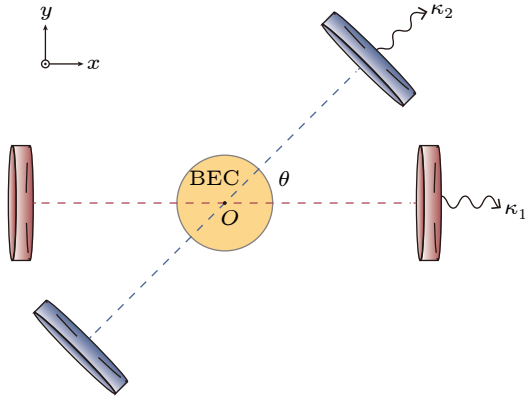

Fig. 1. A 2D BEC trapped inside two cavities placed in the x–y plane, and driven by the pumping beam applied along the z direction. The cavity along the x direction is labeled by cavity 1 with decay rate κ_1 (red), while the one placed at an angle of θ is cavity 2 with decay rate κ_2 (blue).

We use the mean-field method and assume that the system reaches a steady state with $\alpha_j \equiv \langle\hat{a}_j\rangle$ after a long enough time. The bracket is defined as $\langle\cdot\rangle = {\rm Tr}\,(\hat{\rho}_{\rm st}\cdot)$, with the steady state density matrix $\hat{\rho}_{\rm st} = e^{-\beta\hat{\mathcal{H}}_0(\alpha_1,\,\alpha_2)}/\mathcal{Z}\otimes|\alpha_1,\,\alpha_2\rangle\langle\alpha_1,\,\alpha_2|$. In this definition, the cavity field coherent state $|\alpha_1,\,\alpha_2\rangle$ obeys $\hat{a}_j|\alpha_1,\,\alpha_2\rangle = \alpha_j|\alpha_1,\,\alpha_2\rangle$, $\beta = 1/T$ is the inverse temperature, $\hat{\mathcal{H}}_0(\alpha_1,\,\alpha_2) = \langle\alpha_1,\,\alpha_2|\int d\boldsymbol{r}\hat{\Psi}^{\dagger}(\boldsymbol{r})\hat{H}_0\hat{\Psi}(\boldsymbol{r})|\alpha_1,\,\alpha_2\rangle$, and the partition function $\mathcal{Z} = {\rm Tr}\,(e^{-\beta\hat{\mathcal{H}}_0(\alpha_1,\,\alpha_2)})$. The dynamical equation for cavity fields follows $i\partial_t\alpha_j = \langle[\hat{a}_j,\,\hat{H}]\rangle - i\kappa_j\alpha_j$. For a steady state, the condition $\partial_t\alpha_j = 0$ leads to

$$(\tilde{\Delta}_{{\rm c}j} + i\kappa_j)\alpha_j - U_0\sum_{l\neq j}B_{jl}\alpha_l = \eta_0\Theta_j, \tag{3}$$

where κ_j is the loss rate of the j-th cavity, and $\tilde{\Delta}_{{\rm c}j} = \Delta_{\rm c} - U_0B_{jj}$ is the effective detuning. Both Θ and B are bosonic density orders defined as $\Theta_j = \int d\boldsymbol{r}\cos(\boldsymbol{k}_j\cdot\boldsymbol{r})n(\boldsymbol{r})$ and $B_{jl} = \int d\boldsymbol{r}\cos(\boldsymbol{k}_j\cdot\boldsymbol{r})\cos(\boldsymbol{k}_l\cdot\boldsymbol{r})n(\boldsymbol{r})$, respectively. The local atomic density is $n(\boldsymbol{r}) = \langle\hat{\Psi}^{\dagger}(\boldsymbol{r})\hat{\Psi}(\boldsymbol{r})\rangle$.

A self-consistent solution of the steady state Eq. (3) can be achieved as follows. Given a predetermined set of $\{\alpha_1,\,\alpha_2\}$, $n(\boldsymbol{r})$ can be obtained by solving the eigen-problem of $\hat{H}_0(\alpha_1,\,\alpha_2)$. Subsequently, we calculate the bosonic density orders and rely on Eq. (3) to acquire the updated $\{\alpha_1,\,\alpha_2\}$. Iterating the aforementioned process until convergence enables the attainment of the steady state of the system. To address the eigen-problem of $\hat{H}_0(\alpha_1,\,\alpha_2)$, the Bloch theorem is applied and the eigenstate of $\hat{H}_0$, denoted as $\psi_{\boldsymbol{k}}(\boldsymbol{r})$, satisfies $\hat{H}_0(\alpha_1,\,\alpha_2)\psi_{\boldsymbol{k}}(\boldsymbol{r}) = \varepsilon_{\boldsymbol{k}}\psi_{\boldsymbol{k}}(\boldsymbol{r})$, with $\boldsymbol{k}$ being the quasi-momentum and $\varepsilon_{\boldsymbol{k}}$ the corresponding eigenvalue. The Bloch wave functions $\psi_{\boldsymbol{k}}(\boldsymbol{r})$ can be expanded as

$$\begin{aligned}\psi_{\boldsymbol{k}}(\boldsymbol{r}) &= e^{i\boldsymbol{k}\cdot\boldsymbol{r}}u_{\boldsymbol{k}}(\boldsymbol{r})\\ &= e^{i\boldsymbol{k}\cdot\boldsymbol{r}}\sum_{l_1,l_2=-l_{\rm c}}^{+l_{\rm c}}\frac{1}{\sqrt{S}}e^{i(l_1\boldsymbol{k}_1+l_2\boldsymbol{k}_2)\cdot\boldsymbol{r}}C_{\boldsymbol{k}}(l_1,\,l_2)\\ &= \sum_{l_1,l_2=-l_{\rm c}}^{+l_{\rm c}}\phi_{\boldsymbol{k},l_1,l_2}(\boldsymbol{r})C_{\boldsymbol{k}}(l_1,\,l_2).\end{aligned} \tag{4}$$

Here, $u_{\boldsymbol{k}}(\boldsymbol{r})$ is a periodic function and can be expanded by plane waves, S is the system area, and $(l_1,\,l_2)$ are integers within the range of $[-l_{\rm c},\,l_{\rm c}]$ with $l_{\rm c}$ the cutoff. We can reorganize the second line into the form of the third line, which expands $\psi_{\boldsymbol{k}}(\boldsymbol{r})$ under a new set of orthogonal complete basis $\{\phi_{\boldsymbol{k},\,l_1,\,l_2}(\boldsymbol{r})\}$ with corresponding coefficients $C_{\boldsymbol{k}}(l_1,\,l_2)$. The matrix element of $\hat{H}_0(\alpha_1,\,\alpha_2)$ under the new basis is

$$H_{0;\boldsymbol{k}}^{l_1',l_2';l_1,l_2} \equiv \int d\boldsymbol{r}\phi_{\boldsymbol{k},l_1',l_2'}^{*}(\boldsymbol{r})\hat{H}_0(\alpha_1,\,\alpha_2)\phi_{\boldsymbol{k},l_1,l_2}(\boldsymbol{r}). \tag{5}$$

Through the diagonalization of $\hat{H}_0(\alpha_1,\,\alpha_2)$, we can determine the coefficients $C_{\boldsymbol{k}}(l_1,\,l_2)$. For simplicity, we assume that the atomic gas is at zero temperature. Now the local atomic density is denoted as $n(\boldsymbol{r}) = N_{\rm at}|\psi_{\rm g}(\boldsymbol{r})|^2$, with $N_{\rm at}$ being the atom number, and $\psi_{\rm g}(\boldsymbol{r})$ is the ground state of $\hat{H}_0(\alpha_1,\,\alpha_2)$ corresponding to $\boldsymbol{k} = 0$.

Phase Diagram and Photon Current. Now, we discuss the influence of cavity loss rates on superradiant phase transitions. For definiteness, we consider an angle of $\theta = \pi/4$ as a typical example. Choosing different angles will not affect any qualitative findings discussed below. However, a larger angle can suppress the superradiance transition as the two superradiance lattices overlap less. In this double-cavity system, there can exist two optical lattices associated with each cavity, and the atoms are interacted with an effective two-dimensional lattice. If the

two cavities are identical with the same loss rate $\kappa_1 = \kappa_2$, the superradiant transition takes place at the same pumping strength and the lattice depths are identical. However, in the case of unequal loss rates $\kappa_1 \neq \kappa_2$, in principle the two cavities experience superradiant transition at different critical pumps, and the number of photons in cavities are in general different. In the following discussion, we denote $\Delta\kappa = \kappa_2 - \kappa_1$ as the disparity in loss rates and assume $\kappa_2 \geq \kappa_1$ without loss of generality.

The self-consistent solution of Eq. (3) for typical choices of pumping parameters η_0/E_r is shown in Fig. 2(a), as a function of $\Delta\kappa$. Apparent deviation is observed in the photon mean-field amplitude $|\alpha_j|$ in cavity 1 (solid line) and cavity 2 (dashed line) for all cases of $\Delta\kappa \neq 0$. By gradually increasing κ_2 while fixing κ_1, the photon number in cavity 2 diminishes until jumping to zero at a critical value κ_{2c}. During this process, the photon number in cavity 1 also reduces monotonically, but jumping to a finite value $|\alpha_1|_s$ beyond κ_{2c}. This result suggests that the transition at κ_{2c} is of first order.

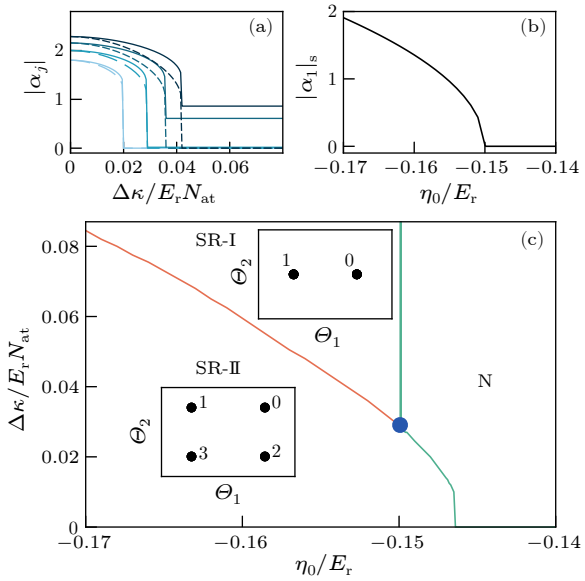

Fig. 2. (a) The mean field photon amplitudes of cavity 1 ($|\alpha_1|$, solid lines) and cavity 2 ($|\alpha_2|$, dashed lines) as functions of the cavity loss rate difference $\Delta\kappa/E_rN_{at}$, under different effective pump strengths $\eta_0/E_r = -0.148, -0.150, -0.152, -0.154$ from bottom to top. (b) The mean field photon amplitude of cavity 1 as a function of effective pumping strength η_0/E_r. (c) The phase diagram in terms of the cavity loss rate difference $\Delta\kappa/E_rN_{at}$ and the effective pumping strength η_0/E_r. Thin and thick solid lines depict second-order and first-order phase transitions, respectively, which join at the tetra-critical point (solid dot). Insets show the symmetry of bosonic density orders (Θ_1, Θ_2) of SR-I and SR-II phases. Here, $U_0/E_r = -10^{-2}$, $\kappa_1/E_rN_{at} = 10^{-3}$, and $\Delta_c/E_rN_{at} = -10^{-1}$.

The reduction of the number of photons in cavity 2 can be easily understood as its loss rate κ_2 increases. However, since cavity 1 is remained unchanged, the decrease in the number of photons therein implies the existence of a photon current flowing from cavity 1 to cavity 2. We delve into the detailed discussion of photon current later. One interesting finding is that while both cavities have fewer photons with increasing $\Delta\kappa$, the difference between them also gets enlarged until reaching a maximum at the first-order transition. By further increasing $\Delta\kappa$, or equivalently κ_2, beyond the transition, the photon number of cavity 1 remains a constant of $|\alpha_1|_s$. In other words, as cavity 2 reaches the normal phase and loses coherence, it no longer affects the superradiance phase of cavity 1, which can only be changed by the effective pump strength and vanishes at a critical η_0, as shown in Fig. 2(b). This transition to the normal phase is companied by a smooth transition of photon number, hence is of second order.

In Fig. 2(c), we map out the phase diagram of the system by varying η_0 and $\Delta\kappa$. Three phases can be identified by characteristic properties of cavity photons, including a normal phase (N), a mixed phase with cavity 1 in superradiance and cavity 2 in normal state (SR-I), and a region where two cavities are both superradiant (SR-II). In the SR-II phase with $|\alpha_1| \geq |\alpha_2| > 0$, the atoms exhibit a quadruple degeneracy with order parameters chosen as (Θ_1, Θ_2), $(-\Theta_1, \Theta_2)$, $(\Theta_1, -\Theta_2)$, and $(-\Theta_1, -\Theta_2)$. In the order parameter space, the four states are labeled as 0, 1, 2, and 3 as depicted in the insert of Fig. 2(c). For the SR-I phase, a self-organized optical lattice emerges only in cavity 1 but not in cavity 2, characterized by $|\alpha_1| > |\alpha_2| = 0$. A double degeneracy is present for states $(\Theta_1, 0)$ and $(-\Theta_1, 0)$, labeled by 0 and 1 as in the insets of Fig. 2(c). This analysis again suggests that the phase transition between SR-I and SR-II (thick red solid line) is a first-order phase transition companied by the change of discrete symmetry and a sudden change of superradiance order parameters. The transition between SR-I (SR-II) and N phase (thin green solid lines) is continuous and characterized by spontaneous breaking of $U(1)$ phase symmetry of photon. The first- and second-order transition lines meet at the tetra-critical point, labeled by the blue dot in Fig. 2(c).

Another unique feature of the SR-II phase is the presence of photon current flowing from cavity 1 to cavity 2. Within the mean-field framework, the net photon current of the steady state is defined as

$$\mathcal{J} \equiv i\langle \hat{a}_2^\dagger \hat{a}_1 - \hat{a}_2 \hat{a}_1^\dagger \rangle = 2\sqrt{N_1 N_2}\sin(\delta\varphi), \tag{6}$$

with $N_j = |\alpha_j|^2$ being the photon number of cavity j and $\delta\varphi = \varphi_2 - \varphi_1$ the phase difference between two cavity fields. The sign of $\mathcal{J}$ indicates the direction of the net photon current. In Fig. 3(a), we present the photon current as a function of the cavity loss rate difference for different effective pumping strengths. One can easily find that the photon current vanishes at $\Delta\kappa = 0$, since the steady-state solution gives $|\alpha_1| = |\alpha_2|$ in this balanced case. Meanwhile, the photon current is also zero at the transition between SR-I and SR-II phases, which can be seen through a comparison of Figs. 2(a) and 3(a). Thus, it is obvious that $\mathcal{J}$ must be a non-monotonic function of $\Delta\kappa$. Numerical solutions given in Fig. 3(a) show that the photon current

reaches a maximal point in the middle of the SR-Ⅱ phase. This observation is caused by the competition between the deduction of total photon numbers with increasing decay rate in cavities 1 and 2, and the increase of photon phase difference $\delta\varphi$. As shown Fig. 3(b), the phase difference $\delta\varphi$ shows an approximate linear dependence on $\Delta\kappa$, and the results almost coincide for all pumping strengths. The variation of $\delta\varphi$ thus leads to a linear behavior of photon current $\mathcal{J}$ for small $\Delta\kappa$, where the total photon number is nearly a constant, and $\delta\varphi$ is small so that $\sin(\delta\varphi) \approx \delta\varphi$. By substituting the steady state equation into Eq. (6), we can expand the photon current to the first order of $\Delta\kappa$ and obtain the following expression

$$\mathcal{J} \approx -\frac{2\tilde{\Delta}_{c1}\eta_0^2\Theta_1\Theta_2\Delta\kappa}{(\tilde{\Delta}_{c1}+\tilde{\Delta}_{c2})^2\kappa_1^2+(\tilde{\Delta}_{c1}\tilde{\Delta}_{c2}-\kappa_1^2-(U_0B_{12})^2)^2}, \tag{7}$$

where the effective detuning $\tilde{\Delta}_{cj}$ and bosonic density order B_{12} are defined as in Eq. (3). This analytic result (dashed lines) is compared with the numerical results of steady state (solid lines), as shown in Fig. 3(a).

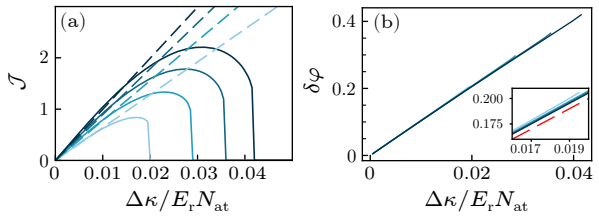

Fig. 3. (a) The net photon current $\mathcal{J}$ (solid lines) as a function of the cavity loss rate difference $\Delta\kappa/E_rN_{at}$, under different effective pumping strengths $\eta_0/E_r = -0.148$, -0.150, -0.152, -0.154 from bottom to top. The current shows linear behavior at small $\Delta\kappa$, and the slope can be analytically extracted (dashed lines). (b) The phase difference $\delta\varphi$ between the two cavities. Results with different effective pumping strengths almost coincide, especially for small $\Delta\kappa$. When $\Delta\kappa$ becomes larger, deviation among these curves, and from a perfect linear behavior (red dashed) can be witnessed in the inset. Parameters used here are the same as those in Fig. 2.

Discussion and Conclusion. Before concluding, we discuss possible experimental realization and detection of the findings mentioned above. The superradiance of BECs in two cavities has been achieved in experiments,[11,12,14] hence the setup proposed in this work can be readily implemented and the superradiant transition can be detected by measuring the photons leaked from the cavities. The characteristic photon current flowing between the two cavities, and its non-monotonic dependence on decay rate can be difficult to measure directly. Instead, the magnitude of each cavity mode can be inferred by counting photon leakage and relying on input-output relation, and the phase difference can be extracted from interference measurement. By substituting the information of mode amplitudes and phase difference into the definition Eq. (6), we can obtain the intra-cavity photon current.

Another factor that usually presents in realistic experiment but not considered here is the inter-atomic interaction. The atomic interaction will modify the ground state of the BEC and induce various types of quantum fluctuations, especially in the strong interaction case. A precise discussion on the impact of atomic interaction is very complicated and surely beyond the scope of the present work. However, for the limit of weak interaction where the quantum fluctuations are negligible, we can obtain some qualitative conclusions. Since an attractive interaction may destroy the BEC, in the following we consider a weak repulsive interaction, and point out that the case of attractive interaction can be analyzed analogously. In general, the presence of a repulsive interaction tends to increase the BEC wave function in spatial dimensions. For the specific problem considered here, the on-site Wannier function of superradiant lattice becomes extended and overlaps more with nearest neighbors. This leads to a larger hopping parameter, or equivalently, a smaller effective mass and higher kinetic energy of fermions. Further, for a given depth of superradiance lattice, an extended Wannier function will increase the atomic potential energy as the wave packet is less confined at the potential well minimum. Finally, after the superradiance transition, the atomic density distribution becomes non-uniform, hence increase the interaction energy compared to the normal phase with a uniform density. As a whole, one would expect that a repulsive interaction can suppress the occurrence of superradiance owing to the three reasons mentioned above.

In summary, we study the superradiant phase transition of a 2D BEC in a cross-aligned double cavity. Within a mean-field treatment, we map out the steady state phase diagram by varying the cavity decay rates and pumping strength. Two superradiant phases are observed and separated by a first-order phase transition, including the SR-I phase with one cavity in superradiance and the other in normal, and the SR-Ⅱ phase with both cavities in superradiance. In the SR-Ⅱ phase, a characteristic net photon current is observed flowing from the cavity with smaller decay rate to the cavity with larger decay rate. The current amplitude shows a non-monotonic dependence on the cavity rate difference, owing to the competition between effects induced by the enhancement of photon number difference and the increase of phase difference. Our findings can be readily realized and measured in experiment.

Acknowledgments. This work was supported by the National Key R&D Program of China (Grant No. 2022YFA1405300), the National Natural Science Foundation of China (Grant Nos. 11734010, 12074428, 12174358, and 92265208), and NSAF (Grant No. U2330401).

References

[1] Brennecke F, Donner T, Ritter S, Bourdel T, Köhl M, and Esslinger T 2007 *Nature* **450** 268

[2] Ritsch H, Domokos P, Brennecke F, and Esslinger T 2013 *Rev. Mod. Phys.* **85** 553

[3] Mivehvar F, Piazza F, Donner T, and Ritsch H 2021 *Adv. Phys.* **70** 1
[4] Keeling J, Bhaseen M J, and Simons B D 2014 *Phys. Rev. Lett.* **112** 143002
[5] Piazza F and Strack P 2014 *Phys. Rev. Lett.* **112** 143003
[6] Chen Y, Yu Z, and Zhai H 2014 *Phys. Rev. Lett.* **112** 143004
[7] Baumann K, Guerlin C, Brennecke F, and Esslinger T 2010 *Nature* **464** 1301
[8] Zhang X, Chen Y, Wu Z, Wang J, Fan J, Deng S, and Wu H 2021 *Science* **373** 1359
[9] Gopalakrishnan S, Shchadilova Y E, and Demler E 2017 *Phys. Rev. A* **96** 063828
[10] Lang J, Piazza F, and Zwerger W 2017 *New J. Phys.* **19** 123027
[11] Léonard J, Morales A, Zupancic P, Esslinger T, and Donner T 2017 *Nature* **543** 87
[12] Morales A, Zupancic P, Léonard J, Esslinger T, and Donner T 2018 *Nat. Mater.* **17** 686
[13] Wu Z, Chen Y, and Zhai H 2018 *Sci. Bull.* **63** 542
[14] Léonard J, Morales A, Zupancic P, Donner T, and Esslinger T 2017 *Science* **358** 1415
[15] Dogra N, Landini M, Kroeger K, Hruby L, Donner T, and Esslinger T 2019 *Science* **366** 1496
[16] Buča B and Jaksch D 2019 *Phys. Rev. Lett.* **123** 260401
[17] Chiacchio E I R and Nunnenkamp A 2019 *Phys. Rev. Lett.* **122** 193605
[18] Soriente M, Donner T, Chitra R, and Zilberberg O 2018 *Phys. Rev. Lett.* **120** 183603
[19] Ferri F, Rosa-Medina R, Finger F, Dogra N, Soriente M, Zilberberg O, Donner T, and Esslinger T 2021 *Phys. Rev. X* **11** 041046